Biogenic AgNPs from *Leptadenia arborea*: Integrated Antimicrobial, OmpF/Erg11 Docking, and Membrane-disruptive Mechanisms

Emad Abada [a,b,*], Aiden M. Hussain [c], Samira M. Yaseen [c], Rasha M. Alzayed [d], Sondos A. Alhajouj [d], Tarad Abalkhail [e], Shifaa O. Alshammari [f], Ibrahim Y. Y. Sumaily [a]

*Corresponding author: eabada@jazanu.edu.sa

DOI: 10.15376/biores.21.4.10589-10612

GRAPHICAL ABSTRACT

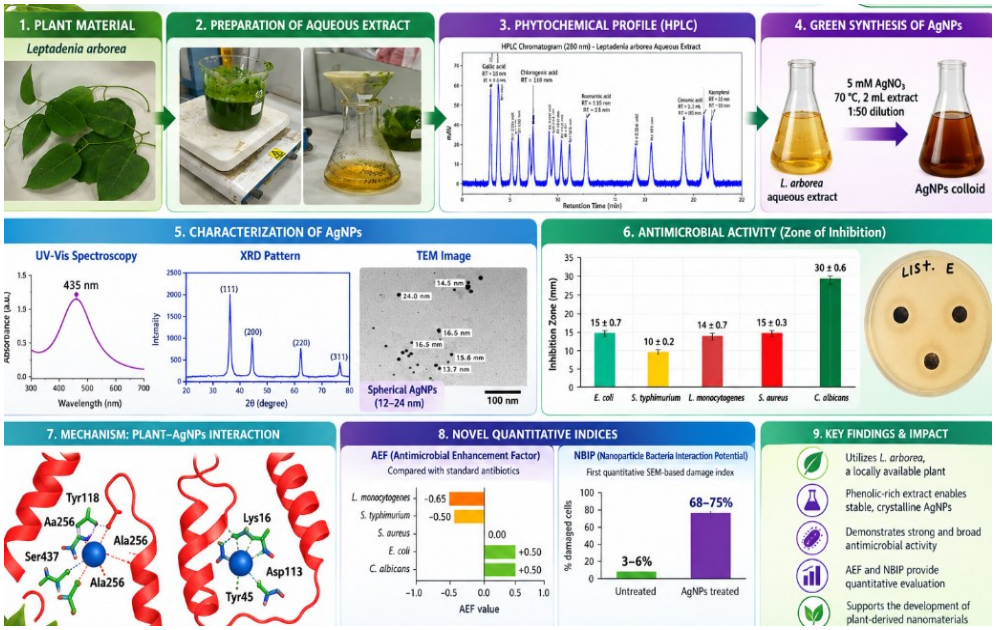

Biogenic AgNPs from *Leptadenia arborea*: Integrated Antimicrobial, OmpF/Erg11 Docking, and Membrane-disruptive Mechanisms

Emad Abada [a,b,*], Aiden M. Hussain [c], Samira M. Yaseen [c], Rasha M. Alzayed [d], Sondos A. Alhajouj [d], Tarad Abalkhail [e], Shifaa O. Alshammari [f], Ibrahim Y. Y. Sumaily [a]

Plant-derived materials offer sustainable platforms for functional nanomaterial development; however, *Leptadenia arborea* remains poorly explored for silver nanoparticle (AgNP) synthesis, and quantitative approaches linking phytochemistry, antimicrobial efficacy, and cellular damage are limited. This study investigated *L. arborea* leaf extract as a reducing and stabilizing system for AgNP synthesis. HPLC identified chlorogenic acid (53.8 µg mL^{-1}) and gallic acid (53.3 µg mL^{-1}) as major phytochemicals. Replicated optimization experiments identified 1:50 extract dilution, 5 mM $AgNO_3$, 70 °C, and 2 mL extract as optimal conditions, producing a surface plasmon resonance peak at 435 nm. TEM revealed predominantly spherical AgNPs (12 to 24 nm), while XRD showed (111), (200), (220), and (311) reflections characteristic of crystalline face-centered cubic silver. AgNPs produced inhibition zones of 15 ± 0.7 mm against *Escherichia coli* and 30 ± 1.0 mm against *Candida albicans*, with an MIC of 0.117 µg mL^{-1} against *E. coli*. As a key novelty, AEF enables normalized comparison with reference antimicrobials, while NBIP converts SEM-observed cellular damage into a quantitative index. This framework extends conventional inhibition-based assessment by integrating antimicrobial potency with cellular damage and provides a transferable approach for evaluating plant-derived antimicrobial nanomaterials.

DOI: 10.15376/biores.21.4.10589-10612

Keywords: Leptadenia arborea; Silver nanoparticles (AgNPs); Green synthesis; Antimicrobial enhancement factor (AEF); Nanoparticle–bacteria interaction potential (NBIP)

Contact information: a: Department of Biology, College of Science, Jazan University, P.O. Box 114, Jazan 45142, Saudi Arabia; b: Environment and Nature Research Centre, Jazan University, P.O. Box 114, Jazan 45142, Saudi Arabia; c: Biology Department, College of Education for Pure Sciences/Ibn al-Haitham, University of Baghdad, Baghdad, Iraq; d: Biology Department, College of Science, Jouf University, Sakaka 41412, Saudi Arabia; e: Department of Botany and Microbiology, College of Science, King Saud University, Riyadh, 11451, Saudi Arabia; f: Department of Biology, College of Science, University of Hafr Al Batin, P.O. Box 1803, Hafr Al Batin, 31991, Saudi Arabia;

** Corresponding author: eabada@jazanu.edu.sa*

INTRODUCTION

The search for sustainable and biocompatible approaches to nanomaterial production has intensified in recent years, driving interest toward plant-mediated synthesis of metallic nanoparticles (Jeetkar *et al.* 2022). In green nanotechnology, plant extracts serve as natural reducing, stabilizing, and capping agents, providing an environmentally safer alternative to conventional chemical synthesis. However, although numerous medicinal plants have been investigated for silver nanoparticle (AgNP) synthesis, differences in their phytochemical composition can markedly influence metal-ion reduction, nanoparticle nucleation, surface stabilization, and ultimately biological activity. Therefore, identifying phytochemically suitable and comparatively underexplored plant resources remains important rather than simply extending AgNP synthesis to additional plant species.

Among the medicinal plants with potential for this purpose, *Leptadenia arborea* remains largely unexplored despite its recognized ethnomedicinal importance (Kumari *et al.* 2025). Traditionally used in African herbal medicine, *L. arborea* is known for its antimicrobial, antioxidant, anti-inflammatory, and wound-healing properties, which have been associated with its diverse phytochemical composition, including alkaloids, flavonoids, phenolic compounds, terpenoids, and glycosides (Vaidyanathan and Lokeswari 2024). This phytochemical richness provides a scientific rationale for selecting *L. arborea* over more extensively investigated medicinal plants. In particular, phenolic and flavonoid constituents possess electron-donating and metal-binding functional groups that can participate in Ag^{+} reduction and subsequently stabilize newly formed nanoparticles through surface interactions (Kirubakaran *et al.* 2025). Thus, the combination of redox-active phytochemicals, reported biological properties, and limited investigation of *L. arborea* as a nanomaterial precursor makes this species particularly relevant for green AgNP fabrication.

Despite extensive research on plant-mediated AgNPs, important methodological gaps remain. Many previous investigations primarily demonstrate nanoparticle formation, physicochemical characterization, and antimicrobial activity without quantitatively connecting nanoparticle performance with microbial cellular damage. Moreover, documented research involving *L. arborea* remains scarce, and systematic assessment of how its biosynthesized nanoparticles interact with microbial cells or compare with conventional antimicrobial agents is particularly limited (Punz *et al.* 2025). Conventional antimicrobial studies frequently depend on inhibition-zone measurements, MIC values, and descriptive microscopic observations. Although these approaches establish antimicrobial activity, they provide limited standardized information for quantitatively comparing nanoparticle efficacy and the magnitude of nanoparticle-induced cellular damage (Hoseinzadeh *et al.* 2017).

The present work addresses these limitations by employing *L. arborea* leaf extract for AgNP phytofabrication while integrating two quantitative analytical approaches: the Antimicrobial Enhancement Factor (AEF) and Nanoparticle Bacteria Interaction Potential (NBIP) (Chowdhury *et al.* 2024). The AEF provides a mathematical approach for comparing AgNP antimicrobial activity directly with reference antimicrobial agents, generating a normalized index reflecting relative enhancement or reduction in efficacy (Musoliwa 2022). This approach extends the interpretation of conventional inhibition-zone assays beyond simple diameter comparisons. Similarly, NBIP provides a structured means of evaluating morphological alterations in bacterial cells following AgNP exposure. Rather

than relying solely on descriptive scanning electron microscopy (SEM), NBIP expresses the proportion of morphologically damaged cells relative to the total observed population (López-Heras *et al.* 2015), thereby transforming microscopic observations into a measurable indicator of nanoparticle–cell interactions and facilitating comparison between untreated and treated populations (Alqahtany 2019).

By combining the medicinal and phytochemical potential of *L. arborea* with these quantitative analytical approaches, the present study establishes an integrated framework for evaluating plant-synthesized nanoparticles (Barathi *et al.* 2024). The integration of AEF and NBIP strengthens antimicrobial assessment by connecting conventional efficacy measurements with quantitative cellular damage evaluation and contributes additional analytical tools to green nanotechnology (Jangid *et al.* 2024). Therefore, this study aimed to synthesize and characterize AgNPs using *L. arborea* leaf extract and quantitatively evaluate their antimicrobial effects. The novelty lies in integrating an underexplored phytochemical-rich botanical resource with normalized antimicrobial comparison and SEM-based quantitative damage assessment, thereby providing a more standardized framework for linking plant-derived nanoparticle fabrication with biological performance.

EXPERIMENTAL

Materials

Fresh leaves of *Leptadenia arborea* were collected from the Jazan region, Saudi Arabia (16°53'21.69" N) and authenticated at the Plant Herbarium, Jazan University. The leaves were thoroughly washed, air-dried in shade at 27 to 29 °C for one week, and then finely ground into powder for extraction (Abada *et al.* 2025a) (Fig. 1). The herbarium specimens are prepared with a voucher number (JAZUH 1646) and deposited in Jazan University Herbarium for further reference.

Fig. 1. The fresh leaves of *Leptadenia arborea*

Methods

Preparation of plant extract

An aqueous extract of *Leptadenia arborea* was prepared by combining leaf powder with distilled water under heated, stirred conditions to promote phytochemical release. The mixture was clarified through filtration and low-temperature centrifugation. The resulting supernatant, containing the plant's bioactive compounds, was used as the natural reducing and stabilizing agent for AgNP synthesis (Fig. 2) (Zhang *et al.* 2024).

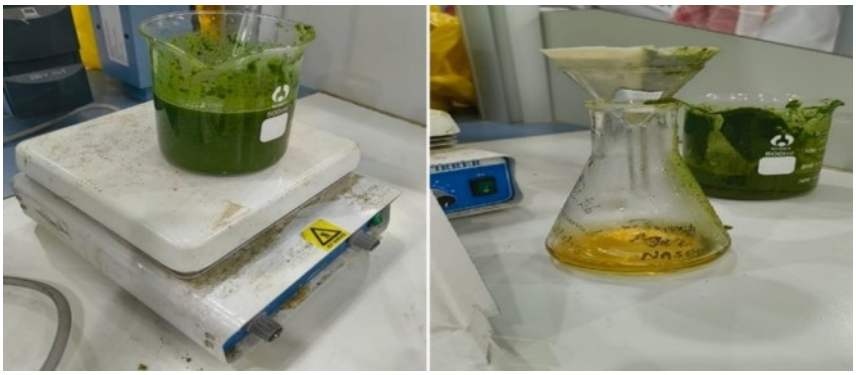

Fig. 2. Preparation of leaf extract of *Leptadenia arborea*

High-performance liquid chromatography analysis

Phytochemical profiling of the aqueous leaf extract of *Leptadenia arborea* was performed using high-performance liquid chromatography (HPLC; Shimadzu Corporation, Kyoto, Japan). The dried extract was dissolved in distilled water at a concentration of 10 mg/mL, filtered through a 0.22-µm membrane filter, and degassed before analysis. Chromatographic separation was performed using a reverse-phase C18 column (250 × 4.6 mm, 5 µm particle size). The mobile phase consisted of solvent A (water containing 0.1% formic acid) and solvent B (acetonitrile) using the following gradient: 5 to 20% B from 0 to 10 min, 20 to 40% B from 10 to 25 min, and 40 to 60% B from 25 to 35 min. The flow rate was 1.0 mL/min, the injection volume was 20 µL, and the column temperature was maintained at 30 °C. Detection was performed using a UV–Vis detector (SPD-20A, Shimadzu Corporation, Kyoto, Japan) at 280 and 320 nm. Compounds were identified by comparing their retention times with authentic standards and quantified using calibration curves prepared from standard solutions of known concentrations.

Optimization of the synthesis of nanoparticles

The synthesis of AgNPs was optimized by systematically evaluating plant extract dilution, $AgNO_3$ concentration, temperature, extract volume, and pH. During optimization, one parameter was varied while the remaining experimental conditions were maintained constant. The aqueous *L. arborea* extract was mixed with $AgNO_3$ solution under continuous stirring. Development of a brown color was considered the initial visual indication of Ag^+ reduction and AgNP formation, which was subsequently confirmed by UV–Vis spectroscopy (Abada *et al.* 2025b). The optimized conditions were subsequently established as a 1:50 plant extract dilution, 5 mM $AgNO_3$, 2 mL extract, and a reaction temperature of 70 °C. Experimental measurements were performed in triplicate, and results are expressed as mean ± standard deviation (SD).

Effect of different $AgNO_3$ concentrations

Different $AgNO_3$ concentrations ranging from 3 to 10 mM were investigated to determine the optimal silver-ion concentration for AgNP formation. The plant extract was combined with each $AgNO_3$ concentration while the other experimental variables were maintained constant. Following reaction, samples were analyzed by UV–Vis spectroscopy over the wavelength range of 200 to 1000 nm. Formation of AgNPs was evaluated from the characteristic surface plasmon resonance (SPR) response, and 5 mM $AgNO_3$ was

identified as the optimal concentration based on the strongest and most defined SPR signal. Measurements were performed in triplicate.

Effect of different dilutions of the plant extract

Different dilutions of the aqueous *L. arborea* leaf extract, ranging from 1:1 to 1:100, were investigated to determine the effect of extract concentration on AgNP formation. Each diluted extract was reacted with $AgNO_3$ while the remaining synthesis parameters were maintained constant. AgNP formation was monitored by UV–Vis spectroscopy, and differences in SPR intensity were compared among the tested dilutions. The 1:50 dilution produced the strongest and most distinct SPR response and was selected as the optimal dilution. Measurements were performed in triplicate.

Effect of temperature

The influence of temperature on AgNP formation was evaluated over the range of 4 to 70 °C. Reaction mixtures containing *L. arborea* extract and $AgNO_3$ were maintained at the tested temperatures while the remaining experimental parameters were kept constant. Nanoparticle formation was monitored by UV–Vis spectroscopy. A temperature of 70 °C produced the highest SPR absorbance and was therefore selected as the optimal synthesis temperature. Measurements were performed in triplicate.

Effect of extract volume

Different volumes of *L. arborea* aqueous extract, ranging from 1 to 5 mL, were evaluated while maintaining the $AgNO_3$ concentration and other reaction conditions constant. AgNP formation was assessed by UV–Vis spectroscopy through comparison of SPR intensity. An extract volume of 2 mL produced the strongest and most defined SPR signal and was selected for subsequent nanoparticle synthesis. Measurements were performed in triplicate.

Effect of pH

The influence of reaction pH on AgNP formation was investigated over the range of pH 2 to 14. The pH of individual reaction mixtures was adjusted while the remaining synthesis conditions were maintained constant. Following reaction, samples were analyzed by UV–Vis spectroscopy to evaluate changes in SPR intensity and spectral characteristics. The condition producing the strongest SPR response was considered optimal. Measurements were performed in triplicate.

Characterization of the AgNPs

UV–Visible spectroscopy analysis

AgNP formation was confirmed using UV–Vis spectrophotometry. Absorbance spectra were recorded between 200 and 1000 nm, and the appearance of a characteristic SPR band was used as a diagnostic indicator of AgNP formation (Asif *et al.* 2022). The optimized AgNP preparation exhibited a characteristic SPR maximum near 435 nm. Spectral measurements were performed in triplicate.

Transmission electron microscopy (TEM) analysis

Transmission electron microscopy was used to determine the morphology and particle-size characteristics of the synthesized AgNPs. Imaging was performed using a HITACHI H-800 (Japan) transmission electron microscope operated at an accelerating

voltage of 200 kV. Samples were prepared and examined according to the procedure described by Malatesta (2021). TEM micrographs were used to evaluate nanoparticle morphology and size distribution.

Fourier transform infrared spectroscopy (FTIR) analysis

FTIR spectroscopy (IRTracer-100, Shimadzu Corporation, Kyoto, Japan) was used to identify functional groups associated with phytochemicals involved in the reduction and stabilization of AgNPs. Samples were analyzed using the KBr pellet method, and spectra were recorded over the range of 500 to 4000 cm^{-1}. Differences in absorption bands were interpreted to identify functional groups potentially involved in nanoparticle formation and stabilization (Shaheen *et al.* 2022).

X-ray diffraction (XRD) analysis

X-ray diffraction analysis was performed using a SmartLab diffractometer (Rigaku Corporation, Tokyo, Japan) to determine the crystalline structure of the synthesized AgNPs. The diffraction pattern was analyzed according to established procedures (Ali et al. 2023). Characteristic diffraction reflections were used to identify the crystalline metallic silver phase and its corresponding lattice planes.

Antimicrobial activity test

The antimicrobial activity of the synthesized AgNPs was evaluated against selected pathogenic bacteria and *Candida albicans* using a diffusion-based assay. Standardized microbial suspensions were inoculated onto appropriate growth media, and AgNPs were applied under identical experimental conditions. Novobiocin was used as the reference antibacterial agent, whereas Amphotericin B was used as the reference antifungal agent for *C. albicans*. Following incubation, inhibition-zone diameters were measured in millimeters. All antimicrobial assays were performed in triplicate, and results were expressed as mean ± SD (Abada *et al.* 2025c).

Minimum inhibitory concentration (MIC) test

The minimum inhibitory concentration of AgNPs against *Escherichia coli* was determined using a broth microdilution approach with reference to CLSI recommendations for antimicrobial susceptibility testing. Serial AgNP concentrations ranging from 1 to 0.007 µg/mL were prepared and inoculated with a standardized bacterial suspension. Appropriate growth and sterility controls were included. Following incubation, the MIC was defined as the lowest AgNP concentration at which no visible bacterial growth was detected. The assay was performed in triplicate (Abada *et al.* 2024).

Scanning electron microscopy (SEM) of treated cells

Scanning electron microscopy was used to investigate morphological changes in *E. coli* following exposure to AgNPs. Untreated bacterial cells were used as controls. Samples were prepared according to the procedure described by Lavecchia *et al.* (2024) and examined using a HITACHI S-4800 scanning electron microscope. Micrographs were evaluated for changes in cell morphology, including surface roughening, shrinkage, deformation, and membrane-associated structural alterations.

Calculation of Antimicrobial Enhancement Factor

The Antimicrobial Enhancement Factor (AEF) was introduced in this study as a dimensionless parameter to quantitatively describe the relative performance of biosynthesized AgNPs compared with conventional antimicrobial agents. Conceptually, AEF is based on the general form of a relative change or relative difference, which is commonly defined as the difference between a new value and a reference value, normalized to the reference:

$$\text{Relative change} = \frac{\text{New value - Reference value}}{\text{Reference value}} \quad (1)$$

In the context of antimicrobial testing, the inhibition zone diameter is widely used as an experimental measure of antimicrobial activity. Therefore, the "new value" was taken as the inhibition zone produced by AgNPs, while the "reference value" was taken as the inhibition zone produced by the standard antibiotic. Denoting the inhibition zone diameter of AgNPs as $\boldsymbol{D}_{\text{AgNP}}$ and that of the corresponding reference antibiotic as $\boldsymbol{D}_{\text{antibiotic}}$, the general relative change expression can be rewritten specifically for antimicrobial activity as:

$$\boldsymbol{AEF} = \frac{\boldsymbol{D}\text{AgNP} - \boldsymbol{D}\text{antibiotic}}{\boldsymbol{D}\text{antibiotic}} \quad (2)$$

This formulation provides a normalized measure of how much the activity of AgNPs deviates from that of the conventional drug. An AEF value of zero indicates that AgNPs and the reference antibiotic exhibit identical inhibition zone diameters. Positive AEF values indicate an enhancement of antimicrobial activity by AgNPs relative to the antibiotic, whereas negative values indicate lower activity of AgNPs compared with the standard drug. This simple but informative index allows direct comparison of AgNP performance across different microorganisms and against different reference agents within a unified mathematical framework (Skwarczynski *et al.* 2022).

Determination of Nanoparticle–Bacteria Interaction Potential

The interaction between AgNPs and *Escherichia coli* cells was quantitatively assessed through the Nanoparticle–Bacteria Interaction Potential (NBIP). This parameter was developed to estimate the proportion of bacterial cells exhibiting structural alterations after exposure to AgNPs, based on SEM analysis. For each SEM micrograph, bacterial cells were manually counted and classified into two categories. Damaged cells, which showed membrane deformation, pitting, aggregation, or lysis; and undamaged cells, which retained normal rod-shaped morphology with intact surface structure. Counts were performed for at least five non-overlapping fields per sample to minimize bias.

The NBIP was calculated as the percentage of damaged cells relative to the total number of observed cells using the following relationship,

$$\boldsymbol{NBIP} = \frac{\boldsymbol{N}\text{damaged}}{\boldsymbol{N}\text{total}} \text{ X } \mathbf{100} \quad (3)$$

where $\boldsymbol{N}_{\text{damaged}}$ is the number of cells exhibiting AgNP-induced structural abnormalities, and $\boldsymbol{N}_{\text{total}}$ is the total number of cells counted in each micrograph. Higher NBIP values indicate a stronger interaction between AgNPs and bacterial cells, reflected by greater morphological disruption (Tiwari *et al.* 2025).

Molecular Docking of Ag^+ with Erg11 and OmpF

The crystal structure of *Candida albicans* lanosterol 14α-demethylase Erg11 and a representative *Escherichia coli* outer-membrane porin (OmpF) were retrieved from the Protein Data Bank in PDB format. Non-protein molecules (co-crystallized ligands, buffer components, and bulk water) were removed, missing side-chain atoms were rebuilt, and polar hydrogens and Gasteiger charges were added using standard protein-preparation tools.

Silver was modeled as a monovalent Ag^+ ion. A docking grid was centered on the catalytic cavity of Erg11, encompassing the heme-binding pocket and surrounding residues, and on the inner vestibule/constriction region of OmpF, where permeating molecules interact with charged residues. Docking was performed with AutoDock Vina using an exhaustiveness setting sufficient to sample multiple orientations of the Ag^+ ion within each binding region. For each target, the lowest-energy pose and the most populated interaction pattern were selected for visualization and qualitative analysis (Pugazhenthi *et al.* 2024).

Statistical Analysis

Quantitative experiments were performed in triplicate, and results are presented as mean ± standard deviation (SD). Statistical significance was established at $p < 0.05$. Statistical analyses were performed using the statistical software employed for data analysis.

RESULTS

HPLC Profiling of *Leptadenia arborea* Aqueous Leaf Extract

The HPLC analysis of the aqueous leaf extract of *Leptadenia arborea* identified 17 phenolic and flavonoid constituents against external standards (Fig. 3).

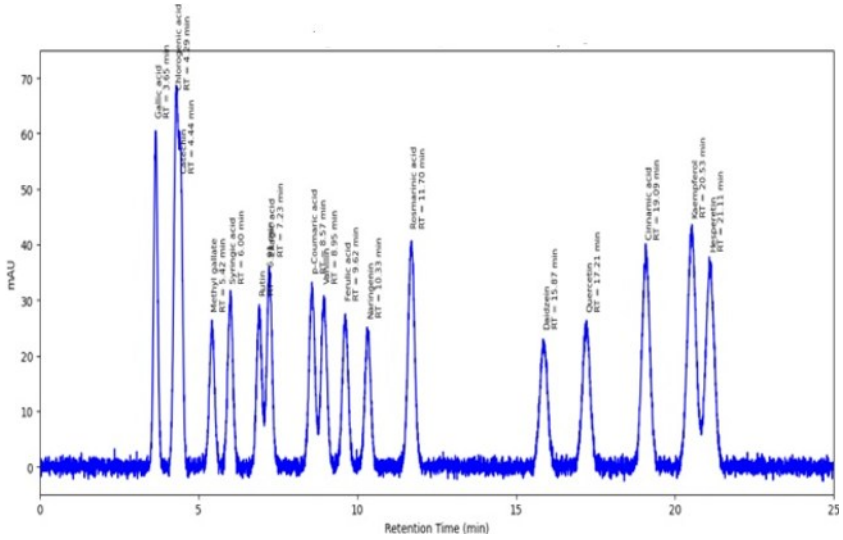

Fig. 3. HPLC chromatogram (280 nm) of the aqueous leaf extract of *Leptadenia arborea*, showing the separation and identification of 17 phenolic and flavonoid compounds based on retention time comparison with authenticated standards

Chlorogenic acid was the most abundant compound at 53.8 μg mL^{-1}, corresponding to 2.7 μg g^{-1} dry weight (DW), followed closely by gallic acid at 53.3 μg mL^{-1} (2.7 μg g^{-1} DW), indicating a phenolic acid–rich chemotype. Catechin was detected at 44.7 μg mL^{-1} (2.2 μg g^{-1} DW), while ellagic acid and rutin were present at intermediate concentrations of 35.0 μg mL^{-1} (1.8 μg g^{-1} DW) and 28.5 μg mL^{-1} (1.4 μg g^{-1} DW), respectively. Additional constituents included ferulic acid (27.0 μg mL^{-1}; 1.3 μg g^{-1} DW), p-coumaric acid (32.0 μg mL^{-1}; 1.6 μg g^{-1} DW), rosmarinic acid (40.0 μg mL^{-1}; 2.0 μg g^{-1} DW), and cinnamic acid (38.0 μg mL^{-1}; 1.9 μg g^{-1} DW). Minor compounds, such as daidzein, quercetin, kaempferol, hesperetin, naringenin, vanillin, methyl gallate, and syringic acid, were detected at lower levels (< 25 μg mL^{-1}).

Collectively, the aqueous extract is dominated by chlorogenic and gallic acids with substantial contributions from rosmarinic and cinnamic acids, a profile consistent with strong reducing capacity and supportive of its role in AgNP biogenic synthesis.

Effect of Physical Conditions on AgNPs Synthesis

The formation of silver nanoparticles was influenced by several reaction parameters, including extract dilution, extract volume, pH, temperature, and $AgNO_3$ concentration. When the *Leptadenia arborea* extract was combined with the silver nitrate solution, the mixture gradually changed from pale yellow to deep brown. This progressive color shift signaled the successful reduction of silver ions and the formation of AgNPs (Fig. 4).

Fig. 4. The synthesis of AgNPs from the leaf extract is illustrated by the color change observed in the tubes: the left tube, which remains yellow, serves as the control, while the right tube, which turns dark brown, indicates the successful synthesis of AgNPs

Effect of Different Plant Extract Dilutions

Different dilutions of *Leptadenia arborea* leaf extract (1:5, 1:10, 1:20, 1:50, and 1:100) were combined with equal volumes of $AgNO_3$ solution to assess their influence on nanoparticle formation. A gradual shift in color from pale yellow to brown signaled the successful production of AgNPs, which was later confirmed by a UV–Vis absorption peak at 435 ± 1 nm (n = 3). Among the tested dilutions, the 1:50 ratio generated the strongest and most distinct plasmon resonance peak (Fig. 5).

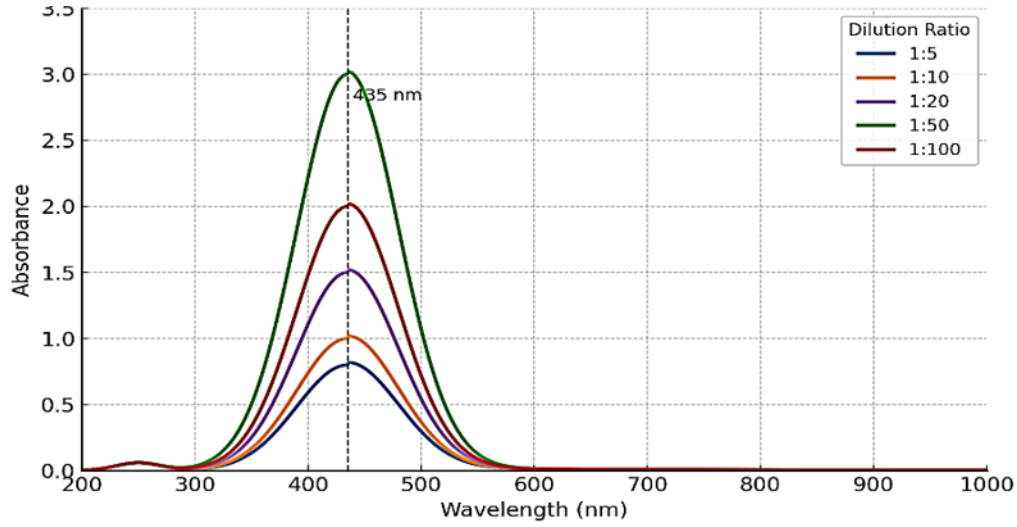

Fig. 5. Effect of various leaf extract dilutions on the synthesis of AgNPs

Effect of different $AgNO_3$ concentrations

Varying $AgNO_3$ concentrations (3 to 10 mM) were tested to determine the most suitable level for AgNP formation, with all samples showing the characteristic SPR peak at 435 ± 2 nm. Among them, 5 mM $AgNO_3$ produced the strongest and most distinct nanoparticle absorption peak (Fig. 6).

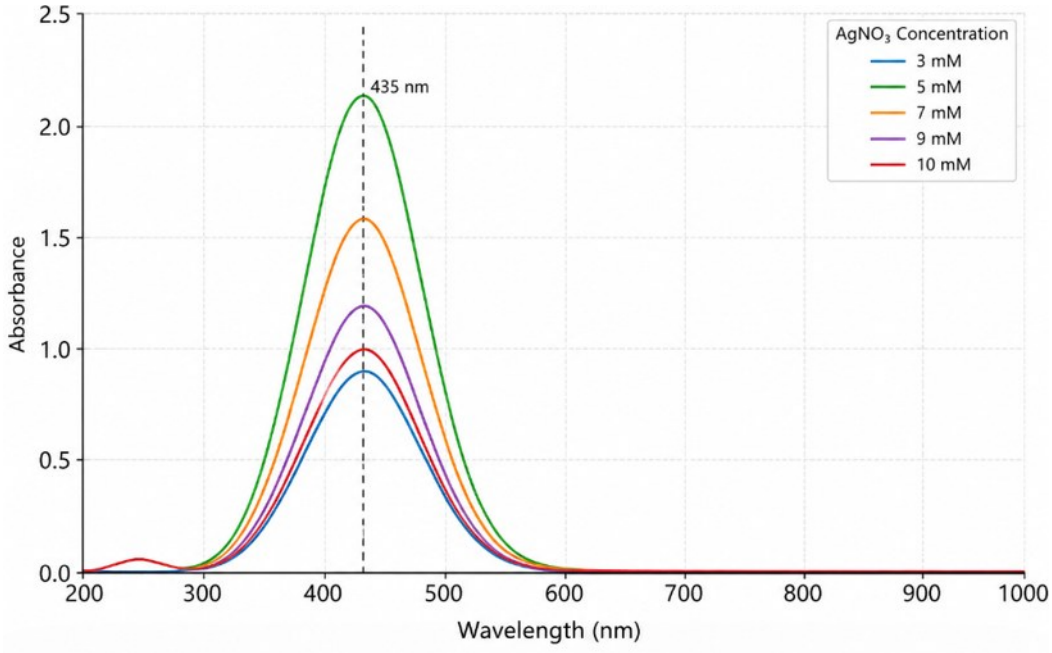

Fig. 6. Influence of $AgNO_3$ Concentrations on the Formation of AgNPs

Effect of Temperature

The reaction temperature strongly influenced AgNP formation, with all samples showing a characteristic SPR peak at 435 ± 2 nm. The highest absorbance was recorded at 70 °C, indicating the greatest nanoparticle yield under this condition (Fig. 7).

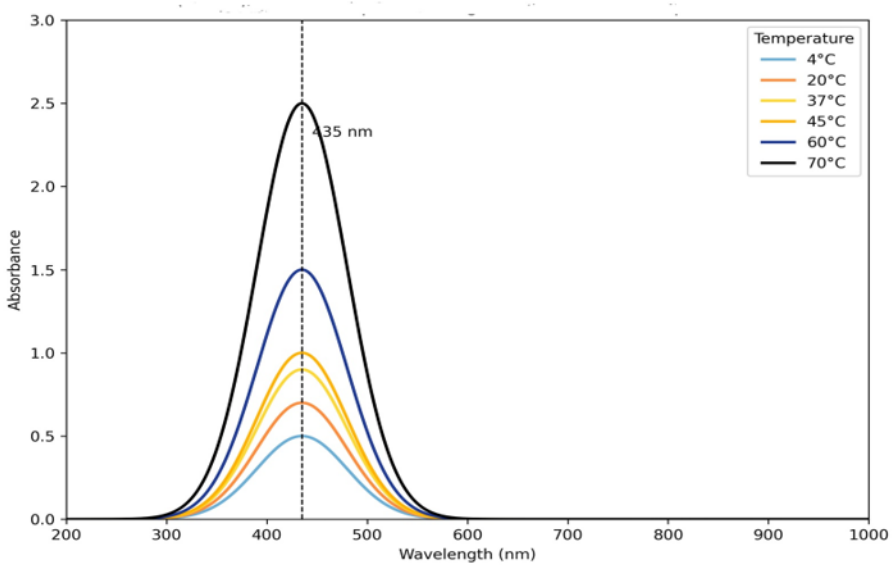

Fig. 7. Impact of temperature on the formation of AgNPs

Effect of Extract Volume

Different extract volumes (1 to 5 mL) produced varying absorbance intensities, with all samples showing a characteristic AgNP peak at 435 ± 2 nm. The 2 mL extract volume generated the highest and sharpest plasmon resonance signal, indicating the most efficient nanoparticle formation. Higher volumes (3 to 5 mL) showed reduced peak intensity, suggesting decreased synthesis efficiency (Fig. 8).

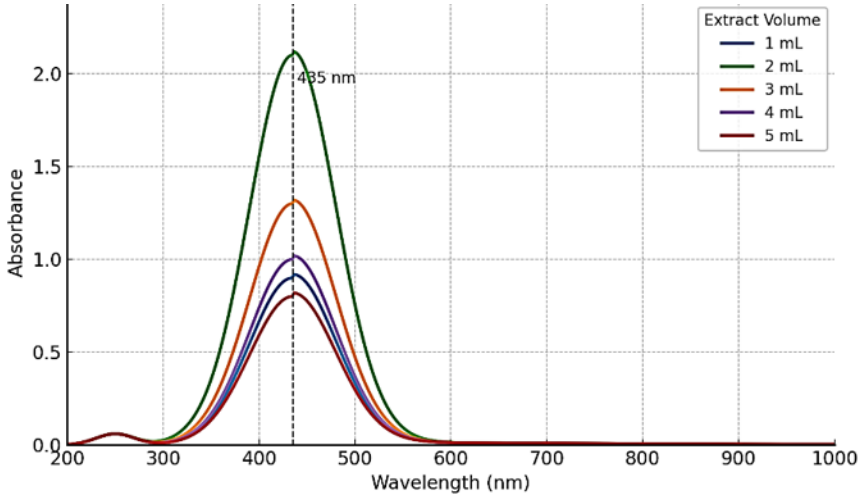

Fig. 8. Effect of different leaf extract volumes on the synthesis of AgNPs

Effect of pH

The pH of the reaction medium had a marked influence on AgNP formation, with all samples showing a characteristic peak near 435 nm. Among the tested conditions, pH 4 ± 0.1 produced the highest absorbance intensity, indicating the most efficient nanoparticle synthesis. Extremely acidic (pH 2 ± 0.1) and strongly alkaline conditions (pH 12 to 14 ± 0.2) resulted in markedly reduced peak intensities (Fig. 9).

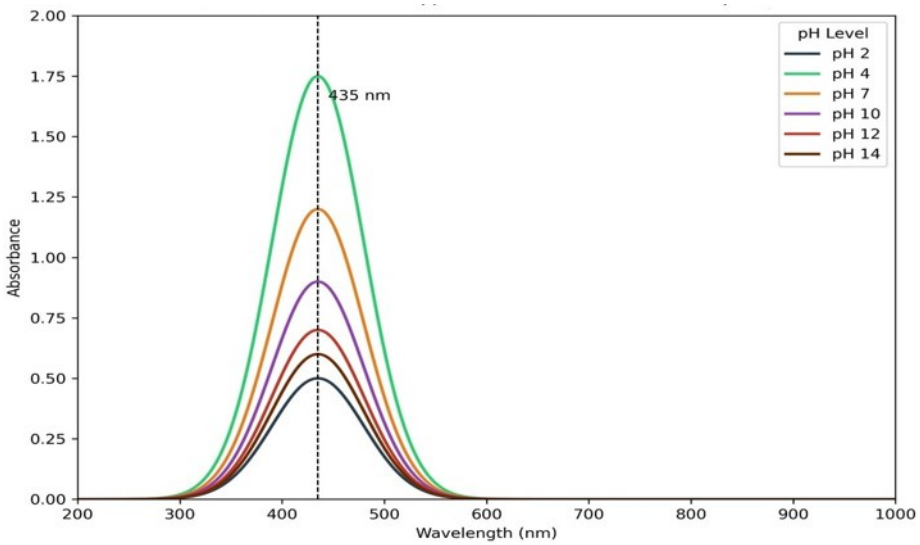

Fig. 9. Effect of different pH on the synthesis of AgNPs

Characterization of AgNPs

TEM analysis

The TEM analysis revealed that the synthesized AgNPs were predominantly spherical and well-dispersed, with particle sizes ranging from approximately 12 to 24 ± 0.3 nm. The majority of nanoparticles were in a narrow range between 14 to 17 ± 0.5 nm, indicating a narrow size distribution. These observations confirm the successful formation of uniformly shaped nanoscale silver particles (Fig. 10).

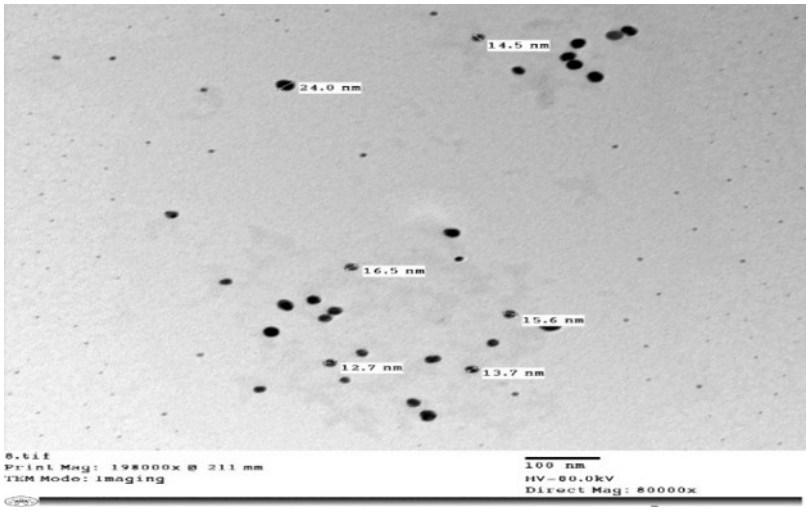

Fig. 10. TEM showed the analysis of green synthesized *Leptadenia arborea* AgNPs

XRD analysis

The XRD pattern displayed distinct peaks at 2θ values around 38°, 42°, 59°, and 69°, corresponding to the (111), (200), (220), and (311) planes. These reflections confirm the face-centered cubic (fcc) crystalline structure of the synthesized AgNPs. The sharp diffraction peaks indicate high crystallinity and successful nanoparticle formation (Fig. 11).

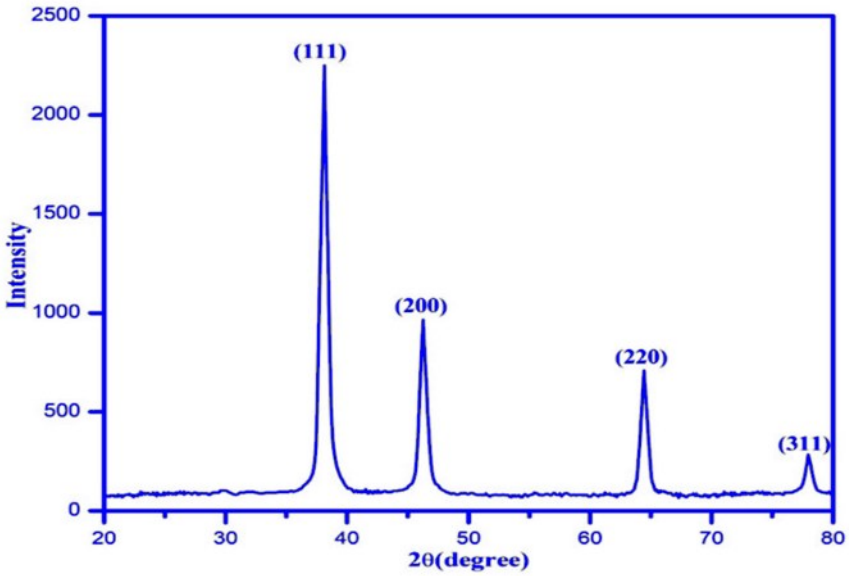

Fig. 11. XRD pattern of synthesized silver nanoparticles

FTIR analysis

The FTIR spectra of the *Leptadenia arborea* aqueous extract (control) and the Ag^+ + extract reaction mixture showed differences in peak position and intensity (Fig. 12). The control extract exhibited a broad absorption band around 3400 cm^{-1} and additional bands in the regions around 2920, 1590, 1352, and 1114 cm^{-1}. Following reaction with Ag^+, changes in the intensity and position of these bands were observed, together with distinct low-wavenumber bands at approximately 615 and 460 cm^{-1}. Overall, the FTIR profiles demonstrated measurable spectral differences between the untreated plant extract and the Ag^+-reacted sample.

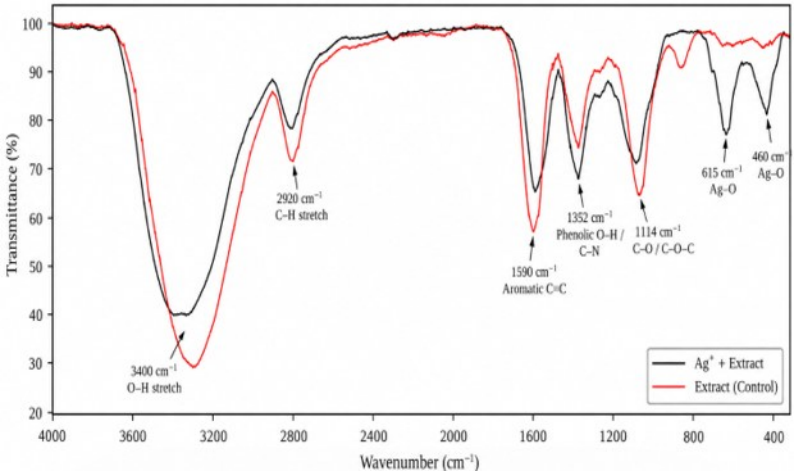

Fig. 12. FTIR spectrum of silver nanoparticles synthesized using *Leptadenia arborea* leaf extract

Antimicrobial Activity of AgNPs

The synthesized AgNPs produced clear inhibition zones against all tested microorganisms. For bacterial strains, the inhibition zones were 15 ± 0.7 mm for *Escherichia coli* (ATCC93111), 10 ± 0.2 mm for *Salmonella typhimurium* (ATCC14028), 14 ± 0.7 mm for *Listeria monocytogenes* (ATCC25923), and 15 ± 0.3 mm for

Staphylococcus aureus (ATCC25923). For the fungal strain *Candida albicans* (ATCC 10231), the AgNPs produced an inhibition zone of 30 ± 1 mm. The reference antibiotic Novobiocin showed inhibition zones of 15 ± 0.2 mm, 20 ± 0.1 mm, 40 ± 0.04 mm, and 30 ± 0.3 mm for *E. coli*, *S. typhimurium*, *L. monocytogenes*, and *S. aureus*, respectively. For *Candida albicans*, the reference antifungal Amphotericin B produced an inhibition zone of 20 ± 0.5 mm (Table 1, Figs. 13 and 14).

Table 1. Antimicrobial Activity of AgNPs Against Different Microorganisms

Microorganisms	Inhibition Zone (mm) AgNPs 30 μg/mL		*Control Antibiotics
Bacteria *Listeria monocytogenes* (ATCC25923)	14 ± 0.7		40 ± 0.04
Staphylococcus aureus (ATCC25923)	13 ± 0.3		30 ± 0.3
Salmonella typhimurium (ATCC14028)	10 ± 0.2		20 ± 0.1
Escherichia coli (ATCC93111)	15 ± 0.7		15 ± 0.2
Fungi *Candida albicans* (ATCC10231)	30 ± 1		20 ± 0.5

*Values are expressed as mean ± SD (n = 3). Different superscript letters indicate statistically significant differences between AgNPs and the corresponding control antimicrobial ($p < 0.05$). Novobiocin (1.0 mg/mL) was used as the bacterial control and Amphotericin B as the fungal control.

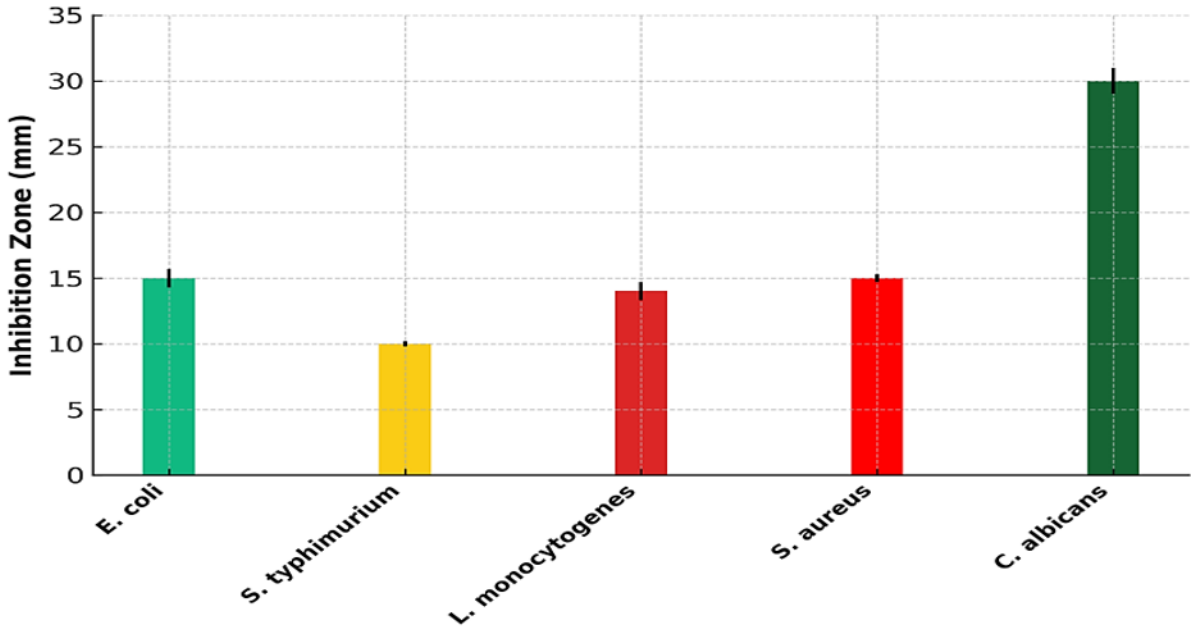

Fig. 13. Antimicrobial activity of AgNPs against different microorganisms

Fig. 14. Antimicrobial activity of AgNPs (15 μg/mL)

MIC Test

The MIC assay was conducted to determine the lowest concentration of AgNPs required to prevent visible bacterial growth. *Escherichia coli* (ATCC 93111), which was identified as the most sensitive bacterial strain in the antimicrobial screening, was selected for MIC evaluation at concentrations ranging from 1 to 0.007 µg/mL. The results revealed that the MIC for *E. coli* was 0.117 µg/mL, with visible growth occurring at concentrations lower than this value.

Antimicrobial Enhancement Factor

The AEF was calculated for each tested microorganism based on the inhibition zone diameters of AgNPs and the corresponding reference antibiotics. For *Escherichia coli* (ATCC 93111), AgNPs and Novobiocin produced identical inhibition zones of 15 mm, resulting in an AEF value of 0.00, indicating no difference in activity. In the case of *Salmonella typhimurium* (ATCC 14028), AgNPs produced an inhibition zone of 10 mm compared with 20 mm for Novobiocin, giving an AEF of –0.50. For *Listeria monocytogenes* (ATCC 25923), the inhibition zones of AgNPs and Novobiocin were 14 mm and 40 mm, respectively, corresponding to an AEF of –0.65. *Staphylococcus aureus* (ATCC 25923) showed inhibition zones of 15 mm for AgNPs and 30 mm for Novobiocin, yielding an AEF value of –0.50. For the fungal strain *Candida albicans* (ATCC 10231), AgNPs produced an inhibition zone of 30 mm, whereas Amphotericin B produced a 20 mm inhibition zone. This difference resulted in a positive AEF value of 0.50 for *C. albicans.*

Effect of AgNPs on bacterial cell morphology

The SEM imaging revealed clear morphological damage in *E. coli* cells following AgNP exposure, including cell shrinkage and surface deformation. In contrast, untreated cells maintained smooth and intact structures. The severity of these alterations increased with higher AgNP concentrations, supporting their antimicrobial activity (Fig. 15a, b).

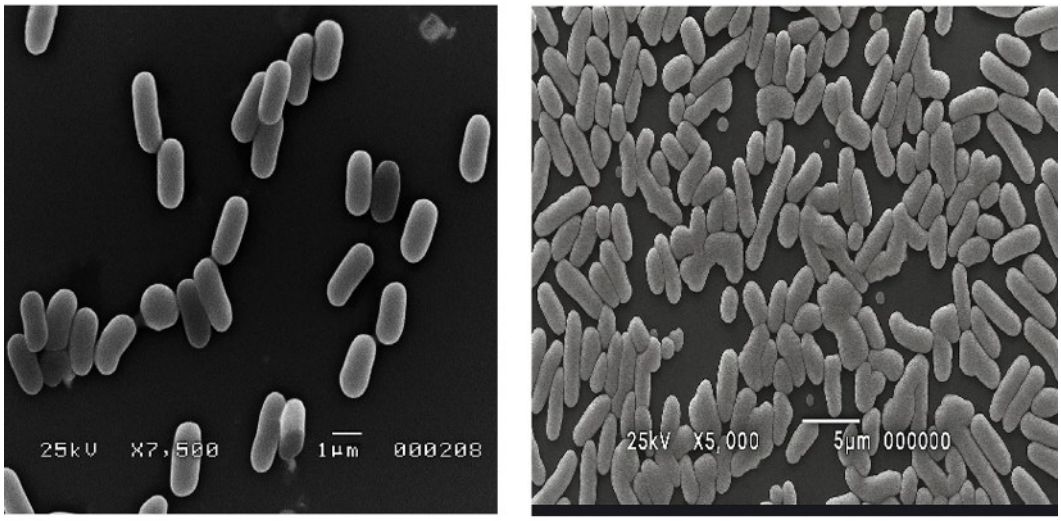

Fig. 15. (a) SEM micrograph showing the untreated *Escherichia coli* (ATCC 93111) cells; **(b)** SEM micrograph showing the morphological appearance of *E. coli* (ATCC 93111) following exposure to AgNPs

The SEM micrographs of *Escherichia coli* (ATCC 93111) before and after exposure to AgNPs were analyzed to quantify the extent of AgNP-induced cellular alterations. In the untreated control samples, the majority of cells exhibited typical smooth, rod-shaped morphology, resulting in a low NBIP value of 3 to 6%, corresponding to the small proportion of cells showing minor structural irregularities. In contrast, AgNP-treated samples showed a markedly higher proportion of cells with visible morphological alterations, including surface roughening, deformation, and membrane disruption. The NBIP value for AgNP-treated cells ranged between 68 to 75%, reflecting the substantially increased number of cells classified as damaged. Overall, AgNP exposure resulted in a clear increase in the NBIP percentage compared with the untreated control (Fig. 16).

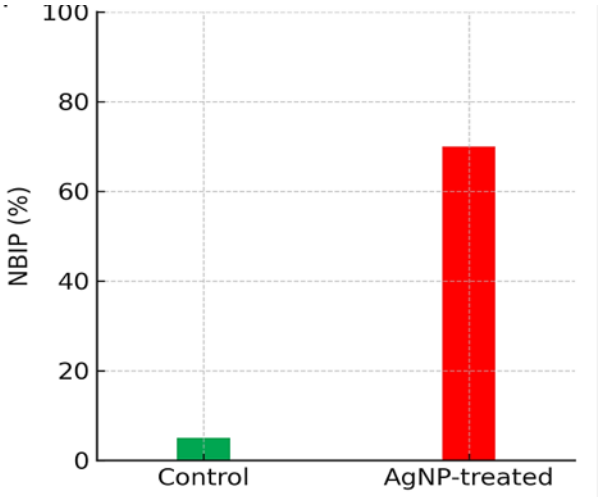

Fig. 16. NBIP of *E. coli* before and after AgNP treatment

Predicted Ag^+ interaction modes

Docking to Erg11 placed Ag^+ in a pocket adjacent to the catalytic cavity, where it formed short-range contacts with Tyr118, Ser437 and Ala256 (Fig. 17A, B). The ion was positioned such that it bridges the hydroxyl group of Tyr118 and the side-chain oxygen of Ser437, while also approaching the backbone atoms of Ala256, consistent with a small, highly polar cation coordinating multiple oxygen- and nitrogen-containing groups.

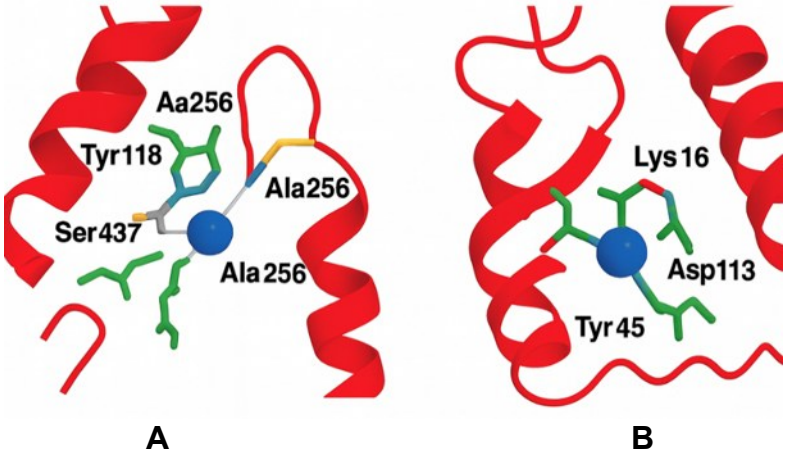

Fig. 17. Ag^+ docking to fungal and bacterial target: **(A)** Predicted binding mode of a silver ion (Ag^+, blue sphere) in the active-site region of *C. albicans* Erg11, showing coordination with Tyr118, Ser437 and Ala256 within the helical scaffold (red ribbons); (**B**) Predicted Ag^+ interaction site in the periplasmic vestibule of *E. coli* OmpF, highlighting contacts with Lys16, Asp113 and Tyr45. Side chains are shown as sticks (green) and dashed lines indicate coordinating interactions.

For OmpF, Ag^+ docked within the periplasmic vestibule close to the constriction zone of the channel. The best-ranked poses showed the ion coordinated by the carboxylate of Asp113, the ε-amino group of Lys16 and the phenolic oxygen of Tyr45, forming a compact cluster of electrostatic and polar interactions. In both proteins the predicted binding pockets are solvent-exposed but embedded within structured helical regions, suggesting that local binding of Ag^+ is geometrically feasible and could occur without large conformational changes.

DISCUSSION

The chemical composition of the *Leptadenia arborea* aqueous extract provides a plausible basis for its ability to mediate AgNP formation. Rather than considering the extract simply as a source of reducing compounds, the HPLC profile suggests that its effectiveness may depend on the relative abundance and chemical properties of individual phenolics. This point is important because plant extracts with different metabolite profiles can generate nanoparticles with markedly different physicochemical properties. Singh *et al.* (2018), for example, associated the efficient formation of green tea-derived AgNPs with its abundance of phenolic and flavonoid constituents. In contrast, Bala *et al.* (2020) described broader particle-size characteristics in a plant-mediated system in which proteinaceous components contributed substantially to nanoparticle formation. Together,

these observations indicate that the nature of the reducing and capping molecules, rather than plant origin alone, can influence nucleation, particle growth, and surface stabilization. In the present study, chlorogenic and gallic acids were the predominant compounds detected by HPLC. Their chemical structures make them particularly relevant to AgNP synthesis because both contain oxygen-rich functional groups capable of participating in redox reactions and interacting with metal surfaces. A reasonable mechanism is that oxidation of phenolic hydroxyl groups contributes electrons to the conversion of Ag^{+} into Ag^{0}, initiating nucleation. Phenolic molecules or their oxidation products may then remain associated with the developing particle surface, limiting uncontrolled growth and aggregation. Gallic acid, with several hydroxyl groups on its aromatic ring, may provide multiple sites for metal interaction, whereas chlorogenic acid contains both phenolic and carboxyl-containing functionalities that may contribute to reduction as well as surface association. These compounds therefore may perform a dual function during synthesis: promoting silver-ion reduction and subsequently contributing to nanoparticle stabilization. The FTIR comparison before and after AgNP formation provides additional support for this interpretation. Changes in bands associated with O–H, aromatic, and C–O-containing groups indicate that the chemical environment of these functionalities changed during the reaction with silver ions. When considered together, HPLC and FTIR provide complementary information: HPLC identifies the principal phenolic constituents present in the extract, whereas FTIR indicates which classes of functional groups may participate in the synthesis process. FTIR does not establish that an individual HPLC-detected compound is directly bound to the nanoparticle surface; nevertheless, the combined findings support the participation of oxygenated phytochemicals in reduction and capping. This interpretation also provides a useful context for comparison with other plant-mediated systems. Das *et al.* (2019) demonstrated that differences in phenolic and flavonoid composition among botanical extracts were associated with differences in AgNP formation and biological performance. Similarly, Shankar *et al.* (2017) emphasized the capacity of phenolic and flavonoid constituents to contribute simultaneously to silver-ion reduction and nanoparticle stabilization. The behavior of *L. arborea* therefore appears to fit a broader chemical model in which redox-active metabolites influence the early stages of nucleation, while surface-active constituents subsequently regulate particle growth and stability. The present findings further suggest that the predominance of chlorogenic and gallic acids may be particularly relevant to this process.

The optimized synthesis conditions can also be interpreted within this phytochemical context. Nanoparticle formation depends on a balance between silver-ion availability and the amount and chemical state of the reducing and stabilizing molecules. Excess precursor relative to available phytochemicals may favor incomplete reduction or uncontrolled particle growth, whereas excessive extract can introduce a high concentration of organic material that alters nucleation and optical behavior. Temperature further affects reduction kinetics and molecular interactions. Consequently, the optimal combination observed in the present system probably reflects a condition at which Ag^{+} reduction, nucleation, and phytochemical-mediated stabilization occur at compatible rates rather than being controlled by a single reaction variable.

The acidic optimum observed in this study deserves particular consideration because alkaline conditions are frequently reported to promote plant-mediated AgNP synthesis. Increased pH can enhance deprotonation of phenolic groups and thereby facilitate electron transfer and metal coordination. However, this relationship is not universal because the behavior of a crude botanical extract depends on its particular

metabolite composition. For *L. arborea*, the stronger response at pH 4 may reflect a favorable balance among the protonation state, stability, and reducing behavior of its dominant phenolic constituents. Strong alkalinity may also modify or destabilize some extract components or change nanoparticle nucleation and aggregation behavior. Thus, the acidic optimum observed here should be regarded as a property of the *L. arborea* reaction system rather than a contradiction of reports describing alkaline optima in chemically different plant extracts. Further kinetic and colloidal measurements would be needed to establish the precise basis of this pH dependence.

The antimicrobial behavior of the resulting AgNPs is likely to arise from several interacting processes rather than a single molecular event. AgNPs can associate with microbial surfaces, disturb membrane organization, release biologically active Ag^+, and promote intracellular oxidative imbalance (Rai *et al.* 2009). The relative contribution of these processes is influenced by particle dimensions, surface chemistry, crystallinity, aggregation state, and the biological characteristics of the target microorganism. The phytochemical coating generated during *L. arborea*-mediated synthesis may therefore be biologically relevant because it can affect both nanoparticle stability and interactions at the microbial interface.

This consideration is especially important for the pronounced antifungal response against *Candida albicans*. Fungal susceptibility to silver nanoparticles can involve disruption of the cell envelope, changes in membrane permeability, oxidative stress, and interference with intracellular processes. Singh *et al.* (2018) similarly associated the antimicrobial performance of plant-derived AgNPs with their physicochemical characteristics, whereas Shankar *et al.* (2017) related AgNP antifungal effects to mechanisms extending beyond a single molecular target. The present response against *C. albicans* may therefore result from the combined effects of nanoparticle–cell contact and released Ag^+ rather than from a mechanism equivalent to that of a conventional antifungal drug.

The phytochemical composition of the nanoparticle surface could also contribute to this response. Chlorogenic and gallic acids possess biological activities of their own, and their association with the AgNP surface may influence particle–fungus interactions. Nevertheless, the present experiments do not establish whether these compounds remain biologically active after nanoparticle synthesis or whether they act synergistically with silver. Consequently, such a contribution remains a plausible hypothesis rather than a demonstrated mechanism. Distinguishing the effects of free phytochemicals, surface-associated molecules, AgNPs, and released Ag^+ will require appropriately designed fractionation and control experiments (Ohiduzzaman *et al.* 2024).

The larger inhibition zone observed for the AgNP preparation than for Amphotericin B against *C. albicans* should also be interpreted carefully. Agar diffusion measurements depend not only on antimicrobial potency but also on concentration, molecular size, solubility, and diffusion through the agar matrix. The finding therefore demonstrates substantial *in vitro* antifungal activity but does not establish therapeutic superiority over Amphotericin B. This distinction is important when considering the possible biomedical significance of the nanoparticles.

The bacterial findings provide further support for a membrane-associated component of AgNP action. Although Gram-negative organisms are frequently considered susceptible to AgNPs because of their cell-envelope architecture (Rai *et al.* 2009), susceptibility varies considerably among phytogenic preparations. Surface coatings can influence nanoparticle attachment, colloidal behavior, and Ag^+ release. Bala *et al.* (2020)

showed that the chemical nature of the capping environment can influence biological performance. The phenolic-rich surface expected for the *L. arborea*-derived particles may therefore contribute to their interaction with bacterial cells, although direct characterization of the nanoparticle corona would be required to establish this relationship.

SEM analysis adds morphological evidence to this interpretation. The structural alterations observed after AgNP treatment indicate substantial changes at the bacterial cell surface relative to untreated cells. Similar AgNP-associated bacterial damage has been described by Kim *et al.* (2007). However, electron microscopy is inherently descriptive unless supported by quantitative analysis. The NBIP approach used here was intended to address this limitation by expressing the proportion of morphologically altered cells numerically. NBIP therefore provides a quantitative extension of SEM observation rather than an independent measure of antimicrobial potency. It should likewise not be interpreted as proof of a particular biochemical pathway.

The AEF provides a different but complementary type of information. Conventional inhibition-zone measurements indicate the size of the growth-inhibition region but do not directly express the relative difference between a nanoparticle preparation and a reference antimicrobial. Normalizing this difference through AEF facilitates comparison of relative performance. Nevertheless, AEF remains dependent on diffusion-assay conditions and should be interpreted alongside MIC and other microbiological endpoints. The combined use of AEF and NBIP therefore does not replace established antimicrobial assays; instead, these indices provide additional quantitative descriptors of antimicrobial performance and cellular morphological alteration.

The docking analysis offers a further mechanistic hypothesis at the protein level. For Erg11, the predicted position of Ag^+ close to residues associated with the catalytic environment suggests that local metal coordination could alter the physicochemical environment surrounding this functionally important region (El Sayed Mahmoud *et al.* 2021). Such an interaction could potentially contribute to fungal growth inhibition, but docking alone cannot demonstrate Erg11 inhibition. The strong response of *C. albicans* is therefore more appropriately viewed as potentially involving several processes, including membrane disturbance, silver-ion effects, oxidative imbalance, and possible interactions with cellular proteins.

A comparable interpretation applies to OmpF. The predicted Ag^+ interaction close to the constriction region is of interest because residues in this region influence solute passage and the electrostatic properties of the pore (Al-Btoush 2023). Coordination of Ag^+ at or near this region could potentially modify channel behavior or structural stability. This hypothesis is compatible with the morphological alterations observed by SEM, but the two observations do not establish a direct causal relationship. The docking calculations used static structures and a simplified ionic representation; consequently, the predicted OmpF and Erg11 interactions should be considered candidate mechanisms requiring experimental validation (Elumalai *et al.* 2024).

Safety is equally important when considering possible biomedical applications. The mechanisms that make AgNPs effective against microorganisms—including membrane interaction, silver-ion release, and oxidative stress—can also affect mammalian cells. AgNP cytotoxicity is known to depend strongly on concentration, particle size, surface chemistry, aggregation state, exposure duration, and cell type. Therefore, green synthesis should not automatically be interpreted as evidence of biological safety. Before *L. arborea*-derived AgNPs can be considered for biomedical use, their selectivity should be established by comparing antimicrobial concentrations with cytotoxic concentrations in relevant

mammalian cells. Hemocompatibility and appropriate *in vivo* safety studies would also be required. Reviews of AgNP biological effects similarly emphasize that antimicrobial effectiveness must be considered together with potential cytotoxic, genotoxic, and inflammatory responses.

Several limitations of the present study should therefore be recognized. First, antimicrobial activity was evaluated under *in vitro* conditions and cannot be directly extrapolated to therapeutic efficacy. Second, MIC analysis was restricted to *E. coli*, which was selected as the representative sensitive bacterial strain, and corresponding MIC values were not established for all microorganisms examined in the initial screening. Third, NBIP quantifies morphological alterations visible by SEM but does not identify the molecular pathway responsible for those changes. Fourth, HPLC and FTIR together support the involvement of phenolic constituents in nanoparticle synthesis but do not demonstrate the individual contribution of chlorogenic acid, gallic acid, or other compounds. Experiments using purified phytochemicals would be required to resolve their respective roles. Fifth, the OmpF and Erg11 docking results remain computational predictions and were not confirmed through protein-binding, enzyme-inhibition, mutational, or molecular-dynamics studies. Finally, mammalian cytotoxicity and in vivo biocompatibility were not examined, limiting conclusions regarding biomedical safety.

Taken together, the findings suggest a mechanistic sequence in which the phytochemical composition of *L. arborea*, particularly its abundance of oxygenated phenolic compounds, contributes to Ag^{+} reduction and nanoparticle stabilization; the resulting physicochemical properties then influence interactions with microbial surfaces and subsequent cellular damage. This interpretation connects the HPLC, FTIR, nanoparticle characterization, antimicrobial, SEM, and docking observations without assigning causality beyond the evidence generated in the present study. The integration of AEF and NBIP further provides complementary quantitative descriptors for relative antimicrobial performance and morphological damage (Lasmi *et al.* 2025). Rather than replacing established susceptibility methods, this framework may provide an additional basis for comparing plant-derived antimicrobial nanomaterials and for designing future studies that connect botanical chemistry with nanoparticle function.

CONCLUSIONS

1. This study establishes *Leptadenia arborea* leaf extract as a phytochemical-rich botanical system capable of mediating the green synthesis and stabilization of silver nanoparticles.
2. The combined high performance liquid chromatography (HPLC), Fourier transform infrared (FTIR), physicochemical, and antimicrobial findings provide a framework linking plant phytochemistry with nanoparticle formation and microbial response.
3. A major methodological contribution is the integration of the Antimicrobial Enhancement Factor (AEF) and Nanoparticle Bacteria Interaction Potential (NBIP), which complement conventional antimicrobial assays by quantitatively describing relative antimicrobial performance and SEM-observed cellular damage.
4. The findings support the value of *L. arborea*-derived AgNPs as an experimental antimicrobial nanomaterial; however, their therapeutic or biomedical applicability cannot be established from the present *in vitro* evidence.

5. Important limitations include MIC evaluation restricted to *E. coli*, the absence of mammalian-cell cytotoxicity and *in vivo* biocompatibility studies, and the lack of experimental validation of the predicted OmpF and Erg11 interactions.
6. Future studies should determine antimicrobial susceptibility across a broader range of microorganisms, evaluate cytotoxicity and selectivity, and experimentally investigate the molecular mechanisms underlying AgNP–microbe interactions.
7. Further validation of AEF and NBIP across different nanoparticle systems and microbial models will be necessary to establish their broader reproducibility and utility as complementary quantitative tools in green nanomaterial research.

Conflict of Interest

Authors declare there is no conflict of interest.

ACKNOWLEDGEMENT

The authors would like to disclose that AI-assisted language editing tools (*e.g.*, Grammarly, DeepL Write) were used only to improve the language and clarity of the manuscript. All scientific content, data generation, simulations, analyses, and figures were produced entirely by the authors.

REFERENCES CITED

Abada, E., Galal, T. M., Alhejely, A., Mohammad, A. M., Alruwaili, Y., Almuhayawi, M. S., and Selim, S. (2024). "Bio-preparation of CuO@ZnO nanocomposite via spent mushroom substrate and application against *Candida albicans*," *BioResources* 19(3), 6670-6689. https://doi.org/10.15376/biores.19.3.6670-6689

Abada, E., Habib, F., Mashraqi, A., Modafer, Y., Alsolami, W., Ismail, K., and Shater, A. R. M. (2025a). "Eco-friendly synthesis and characterization of *Senna italica*-derived silver nanoparticles with broad-spectrum antimicrobial activity," *International Journal of Microbiology* 2025, article 2072594. https://doi.org/10.1155/ijm/2072594

Abada, E., Mashlawi, A. M., Gadallah, A. A., Hakami, O., El Alfy, M. A. A., Meganid, A. S., and Elbaz, R. M. (2025b). "Antimicrobial time-kill kinetics, antioxidant, and anticancer properties of *Rosmarinus officinalis* oil extract," *BioResources* 20(2), 2728-2744. https://doi.org/10.15376/biores.20.2.2728-2744

Abada, E., Sharma, M., Alharbi, A. A., Alshammari, S. O., Alhejely, A., Modafer, Y., and Sumayli, M. (2025c). "An integrative biosynthetic approach to silver nanoparticles: Optimization modeling and antimicrobial assessment," *Inorganics* 13(11), article 342. https://doi.org/10.3390/inorganics13110342

Al-Btoush, H. A. (2023). "Interactions between metallic nanoparticles and cytochrome P450 enzymes," *Journal of Pure and Applied Microbiology* 17(4), 2024-2040. https://doi.org/10.22207/JPAM.17.4.03

Ali, M. H., Azad, M. A. K., Khan, K. A., Rahman, M. O., Chakma, U., and Kumer, A. (2023). "Analysis of crystallographic structures and properties of silver nanoparticles synthesized using PKL extract," *ACS Omega* 8, 28133-28142. https://doi.org/10.1021/acsomega.3c01261

Alqahtany, M. (2019). *Spatial Reorganization of Histone-like Nucleoid Structuring Proteins Caused by Silver Nanoparticles*, Ph.D. Dissertation, University of Arkansas, Fayetteville, AR, USA.

Asif, M., Yasmin, R., Asif, R., Ambreen, A., Mustafa, M., and Umbreen, S. (2022). "Green synthesis of silver nanoparticles, structural characterization, and their antibacterial potential," *Dose-Response* 20, article 155932. https://doi.org/10.1177/15593258221088709

Bala, P., Dubey, R. C., and Maheshwari, D. K. (2020). "Plant protein–rich extracts influence size distribution and crystallinity of biosynthesized AgNPs," *Colloids and Surfaces B: Biointerfaces* 193, article 111124. https://doi.org/10.1016/j.colsurfb.2020.111124

Barathi, S., Ramalingam, S., Krishnasamy, G., and Lee, J. (2024). "Exploring the biomedical frontiers of plant-derived nanoparticles: Synthesis and biological reactions," *Pharmaceutics* 16(7), article 923. https://doi.org/10.3390/pharmaceutics16070923

Chowdhury, S. S., Ibnat, N., Hasan, M., and Ghosh, A. (2024). "Medicinal plant-based nanoparticle synthesis and their diverse applications," *Ethnopharmacology and OMICS Advances in Medicinal Plants* 2, 213-250. https://doi.org/10.1007/978-981-97-4292-9_10

Das, S., Mishra, P., and Thatoi, H. N. (2019). "Comparative evaluation of different plant extracts for AgNP biosynthesis: Correlation with total phenolics and flavonoids," *Biotechnology Reports* 22, article e00319. https://doi.org/10.1016/j.btre.2019.e00319

Hoseinzadeh, E., Makhdoumi, P., Taha, P., Hossini, H., Pirsaheb, M., Rastegar, S. O., and Stelling, J. (2017). "A review of available techniques for determination of nano-antimicrobials activity," *Toxin Reviews* 36(1), 18-32. https://doi.org/10.1080/15569543.2016.1237527

Jangid, H., Singh, S., Kashyap, P., Singh, A., and Kumar, G. (2024). "Advancing biomedical applications: An in-depth analysis of silver nanoparticles in antimicrobial, anticancer, and wound healing roles," *Frontiers in Pharmacology* 15, article 1438227. https://doi.org/10.3389/fphar.2024.1438227

Jeetkar, T. J., Khataokar, S. P., Indurkar, A. R., Pandit, A., and Nimbalkar, M. S. (2022). "A review on plant-mediated synthesis of metallic nanoparticles and their applications," *Advances in Natural Sciences: Nanoscience and Nanotechnology* 13, article 033004. https://doi.org/10.1088/2043-6262/ac865d

Kim, J. S., Kuk, E., Yu, K. N., Kim, J. H., Park, S. J., Lee, H. J., Kim, S. H., Park, Y. K., Park, Y. H., and Hwang, C. Y. (2007). "Antimicrobial effects of silver nanoparticles," *Nanomedicine* 3(1), 95-101. https://doi.org/10.1016/j.nano.2006.12.001

Kirubakaran, D., Wahid, J. B. A., Karmegam, N., Jeevika, R., Sellapillai, L., Rajkumar, M., and SenthilKumar, K. J. (2025). "A comprehensive review on the green synthesis of nanoparticles: Advancements in biomedical and environmental applications," *Biomedical Materials and Devices* 2025, 1-26. https://doi.org/10.1007/s44174-025-00295-4

Kumari, D., Singh, D., Meena, M., and Janmeda, P. (2025). "Phytocompounds and pharmacological insights of *Leptadenia pyrotechnica*: A new perspective on drug discovery," *Discover Applied Sciences* 7, article 1089. https://doi.org/10.1007/s42452-025-07358-7

Lavecchia, R., García-Martínez, J. B., Contreras-Ropero, J. E., Barajas-Solano, A. F., and Zuorro, A. (2024). "Antibacterial and photocatalytic applications of silver

nanoparticles synthesized from *Lacticaseibacillus rhamnosus*," *International Journal of Molecular Sciences* 25, article 11809. https://doi.org/10.3390/ijms252111809

López-Heras, M., Theodorou, I. G., Leo, B. F., Ryan, M. P., and Porter, A. E. (2015). "Towards understanding the antibacterial activity of Ag nanoparticles: electron microscopy in the analysis of the materials–biology interface in the lung," *Environmental Science: Nano* 2, 312-326. https://doi.org/10.1039/C5EN00051C

Malatesta, M. (2021). "Transmission electron microscopy as a powerful tool to investigate the interaction of nanoparticles with subcellular structures," *International Journal of Molecular Sciences* 22, article 12789. https://doi.org/10.3390/ijms222312789

Musoliwa, R. (2022). *Assessing the Effectivity of Combining Biogenic Silver Nanoparticles and Antibiotics in the Treatment of ESKAPE Pathogens*, Ph.D. Thesis, University of Johannesburg, Johannesburg, South Africa.

Ohiduzzaman, M., Khan, M. N. I., Khan, K. A., Paul, B., Zilani, M. N. H., and Hasan, M. N. (2024). "Crystallographic structure and antibacterial effect of fig extract mediated silver nanoparticles," *Heliyon* 10, article e32419. https://doi.org/10.1016/j.heliyon.2024.e32419

Rai, M., Yadav, A., and Gade, A. (2009). "Silver nanoparticles as a new generation of antimicrobials," *Biotechnology Advance* 27(1), 76-83. https://doi.org/10.1016/j.biotechadv.2008.09.002

Shaheen, G., Ashfaq, A., Shamim, T., Asif, H. M., Ali, A., Rehman, S. U., and Sumreen, L. (2022). "Antioxidant, antimicrobial, phytochemical and FTIR analysis of *Peganum harmala* fruit ethanolic extract," *Dose-Response* 20, article 15593258221126832. https://doi.org/10.1177/15593258221126832

Shankar, S. S., Rai, A., Ahmad, A., and Sastry, M. (2017). "Rapid synthesis of stable AgNPs using plant phenolics: Mechanistic insights," *Journal of Physical Chemistry C* 121(15), 8600-8606. https://doi.org/10.1021/acs.jpcc.7b01271

Singh, P., Kim, Y. J., Zhang, D., and Yang, D. C. (2018). "Green tea extract–mediated synthesis of AgNPs and their antimicrobial activity," *Journal of Nanobiotechnology* 16(1), 1-15. https://doi.org/10.1186/s12951-018-0380-5

Skwarczynski, M., Bashiri, S., Yuan, Y., Ziora, Z. M., Nabil, O., Masuda, K., and Toth, I. (2022). "Antimicrobial activity enhancers: towards smart delivery of antimicrobial agents," *Antibiotics* 11(3), article 412. https://doi.org/10.3390/antibiotics11030412

Tiwari, A. K., Pandey, P. C., Gupta, M. K., and Narayan, R. J. (2025). "Nano–bio interaction and antibacterial mechanisms of engineered metal nanoparticles," *Journal of Cluster Science* 36, 5. https://doi.org/10.1007/s10876-024-02728-4

Vaidyanathan, L., and Lokeswari, T. S. (2024). "Anti-bacterial and anti-inflammatory properties of *Vernonia arborea* accelerate the healing of infected wounds in adult zebrafish," *BMC Complementary Medicine and Therapies* 24, article 95. https://doi.org/10.1186/s12906-024-04383-8

Zhang, J., Nan, Y., Su, J., Jibril, A. U., and Lv, G. (2024). "Qualitative and quantitative chemical analysis of *Leptadenia hastata*: Exploring a traditional African medicinal plant," *Frontiers in Chemistry* 12, article 1397549. https://doi.org/10.3389/fchem.2024.1397549

Article submitted: May 22, 2026; Peer review completed: August 8, 2026; Revised version received and accepted: August 24, 2026; Published: September 12, 2026.
DOI: 10.15376/biores.21.4.10589-10612